Available online at www.sciencedirect.com
ScienceDirect
Journal of Power Sources 162 (2006) 606–613
JOURNAL OF POWER SOURCES
www.elsevier.com/locate/jpowsour

Electrochemical properties of $LiNi_{0.5}Mn_{1.5}O_4$ films prepared by spin-coating deposition

José C. Arrebola [a], Álvaro Caballero [a], Lourdes Hernán [a], Montserrat Melero [a], Julián Morales [a,*], Enrique R. Castellón [b]

[a] *Departamento de Química Inorgánica e Ingeniería Química, Campus de Rabanales, Edificio Marie Curie, Universidad de Córdoba, 14071 Córdoba, Spain*
[b] *Departamento de Química Inorgánica, Campus de Teatinos, Universidad de Málaga, Málaga, Spain*

Received 1 February 2006; received in revised form 5 May 2006; accepted 9 June 2006
Available online 27 July 2006

Abstract

Highly uniform films of pure $LiNi_{0.5}Mn_{1.5}O_4$ spinel were obtained by spin-coating stoichiometric amounts of $Mn(CH_3COO)_2$ and $Ni(CH_3COO)_2$ dissolved in de-ionized water, and $Li(i\text{-}OC_3H_7)$ dissolved in a 1:2 CH_3-COOH/i-C_3H_7OH mixture, onto an Au substrate. The resulting gel was transformed into a spinel by calcining at variable temperatures from 400 to 800 °C. The deposits, thus, obtained were characterized by scanning electron microscopy (SEM), and X-ray diffraction and X-ray photoelectron spectroscopy (XPS), and their electrochemical properties determined from potentiostatic and galvanostatic measurements. The spinel formed at 400 °C, with an earthworm-like shape, the origin of which was ascribed to the formation of a layer of undecomposed organic components. At 800 °C, the film exhibited markedly improved in crystallinity and the spinel particles adopted a polyhedral shape of submicron size with well-defined edges and faces, thus, reducing the interparticle connectivity. Nickel atoms were found to occur in two chemical environments, namely: as Ni^{2+} and Ni^{3+}, the former being the major component. The potentiostatic curves obtained were consistent with the spinel formula as they exhibited two well-defined peaks in the 4.6–4.8 V region associated to $Ni^{2+} \rightarrow Ni^{3+} \rightarrow Ni^{4+}$ processes. Also, both potentiostatic curves and galvanostatic curves were consistent with a reversible Li insertion/extraction reaction; however, the cells exhibited significant overcharge that was probably due to electrolyte decomposition catalyzed by gold. The thin deposits obtained were found to deliver capacities around 148 mAh g^{-1} and to efficiently retain them upon extended cycling. However, the coulombic efficiency of the deposits was rather low (around 50% at the 50th cycle). Increasing the film thickness, raised the coulombic efficiency to 85% but decreased the delivered capacity, probably through increased resistance of the electrode; however, capacity retention on cycling was maintained.

Keywords: Spin-coating deposition; Lithium–nickel–manganese spinel; High-voltage lithium batteries

1. Introduction

The trend towards miniaturizing a host of electronic and mechanical devices has raised the demand for small power sources, such as rechargeable Li-ion microbatteries. This has promoted extensive research into thin-film based microbatteries as regards preparation technology and the deposited materials [1–6]. Chemical vapor deposition and sputtering have so far been the most frequently used deposition techniques used [7–10], and $LiCoO_2$ and $LiMn_2O_4$, the cathodic materials most commonly tested [11–15], for this purpose. These materials can afford potentials below 4.5 V. The partial replacement of manganese in $LiMn_2O_4$ with various transition metals is known to endow this compound with the ability to deliver a substantial capacity at voltages above 4.5 V [16–18]. $LiNi_{0.5}Mn_{1.5}O_4$ [19–20] is the doped spinel exhibiting the best electrochemical properties as a result of the nickel (i) being oxidized at a potential below 4.8 V, which is somewhat lower than those for other transition elements, such as Co, Fe or Cu (ca. 5 V), the difference being important because such a high potential can favor unwanted reactions and (ii) exchanging two electrons (from Ni^{2+} to Ni^{4+}), whereas the other elements exchange only one. As a result, the Ni-doped spinel delivers a higher capacity at this potential, which can open up prospects for a new generation of Li-ion

* Corresponding author. Tel.: +34 957 218620; fax: +34 957 218621.
E-mail address: iq1mopaj@uco.es (J. Morales).

0378-7753/$ – see front matter © 2006 Elsevier B.V. All rights reserved.
doi:10.1016/j.jpowsour.2006.06.024

batteries of higher energy than those commercially available at present.

The electrochemical activity of $LiNi_{0.5}Mn_{1.5}O_4$ in thin-film intercalation electrodes prepared by electrostatic spray deposition has been known for a few years [21]. Cell performance was essentially determined from cyclic voltammetry measurements. Although this technique provides valuable information, particularly concerning the different steps of the electrochemical reaction, some characteristics, such as specific charge–discharge capacities, coulombic efficiency and cycle life are better examined by galvanostatic methods. We, recently, reported on the performance of this spinel as a film electrode prepared by electrophoretic deposition [22] in a lithium cell, where it exhibited promising results as regards both delivered capacity and cycle life. The greatest shortcoming encountered was the need to press the active material in order to ensure an adequate electrochemical response. In this work, we used a different approach to prepare thin films of the spinel (viz. a sol–gel method assisted by spin-coating) and studied their structure and electrochemical properties in depth.

2. Experimental

Thin-film $LiNi_{0.5}Mn_{1.5}O_4$ electrodes were prepared by spin-coating a homogeneous precursor solution onto Au substrates 13 mm in diameter. The process is depicted in Fig. 1. Stoichiometric amount of the precursors [$Mn(CH_3COO)_2$ and $Ni(CH_3COO)_2$ dissolved in de-ionized water, and $Li(OC_3H_7^i)$ dissolved in a 1:2 CH_3-COOH/*i*-C_3H_7OH mixture] were mixed with stirring for 6 h. Then, the sol was deposited onto the substrate by using a spin-coater (SCS model G3P-8, supplied by PI-KEM) at 3000 rpm. Once the gel formed, the deposition process was repeated several times in order to ensure that the film thickness would be adequate for electrochemical measurements. The gel was transformed into a spinel at 400, 600 and 800 °C. Although stainless substrates were also tested, their surface was strongly degraded and the spinel composition altered at high temperature. The amount of oxide attached to the substrate was determined by weighing on a Sartorius microbalance sensitive to within ±1 μg before and after deposition.

The textural properties of the films were analyzed by scanning electron microscopy using a Jeol 6400 instrument. X-ray diffraction patterns were recorded on a Siemens D5000 X-ray diffractometer using Cu Kα radiation and a graphite monochromator for the diffracted beam. The scanning conditions were 15°–90° (2θ), a 0.03° step size and 12 s per step. X-ray photoelectron spectra were obtained with a Physical Electronics PHI 5700 spectrometer using non-monochromated Mg Kα radiation ($h\nu$ = 1253.6 eV). Binding energies were corrected using the binding energy values of C(1s) of adventitious carbon (and of the methyl group) fixed at 284.8 eV. Samples were mounted on a holder without adhesive tape and kept under high vacuum in the preparation chamber overnight before they were transferred to the analysis chamber of the spectrometer. Survey spectra over the range 0–1200 eV were recorded at a 187.85 pass energy, each region being scanned several times to ensure an adequate signal-to-noise ratio. Spectra were processed by using PHI-Access V.6 and Multipak software, both from Physical Electronics. High-resolution spectra were fitted following Shirley background correction and satellite subtraction. Surface atomic concentrations were determined from peak areas, using Shirley background subtraction and the sensitivity factors provided by the spectrometer manufacturer (Physical Electronics, Eden Prairie, MN). An Ar^+ ion beam of 4 keV was used for depth profiling and the composition was measured from the integrated intensities of the XPS spectra.

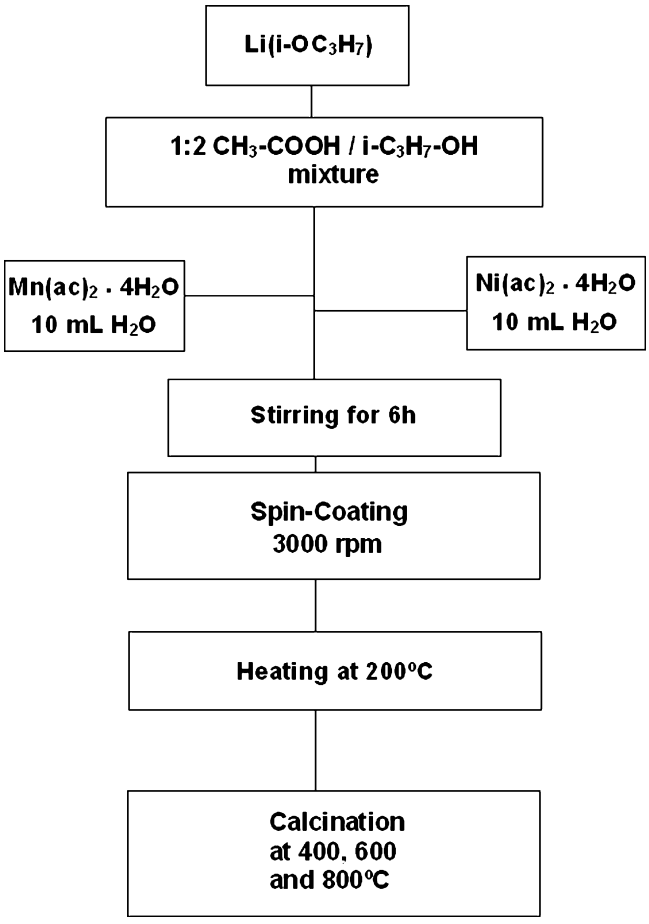

Fig. 1. Procedure for preparing $LiNi_{0.5}Mn_{1.5}O_4$ films by spin-coating.

Electrochemical measurements were made with either two-electrode Swagelock-type or CR2032 coin-type cells, using Li (supplied by Strem) as anode and a piece of Whatman paper as a spacer. The electrolyte, supplied by Merck, was 1 M anhydrous LiPF6 in a 1:1 mixture of ethylene carbonate and dimethyl carbonate. Cells were assembled in an M-Braun glove-box. Step potential electrochemical spectroscopy (SPES) curves were recorded at 2.5 mV per 0.06 h per step. Galvanostatic tests were conducted under a C/2 charge/discharge regime (C representing one Li^+ ion exchanged in 1 h). Both types of electrochemical measurements were performed on a McPile II (Biologic) potentiostat–galvanostat system. All measurements were made at least in duplicate in order to ensure reproducibility in the electrochemical results.

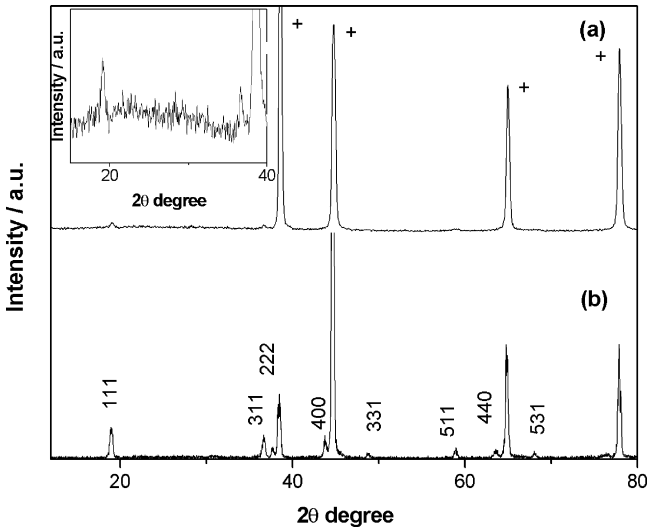

Fig. 2. XRD patterns for spin-coating deposits calcined at: (a) 400 and (b) 800 °C. (+) Substrate.

3. Results and discussion

3.1. Textural and structural properties

Fig. 2 shows the XRD patterns of the films on the Au substrate. All peaks except those for the substrate can be indexed on the spinel structure, which suggests that the deposited material was highly pure. The increase in peak intensity and the decrease in peak broadening with increasing annealing temperature are consistent with improved crystallinity, which, as shown below, has a strong influence on the electrochemical properties. The lattice parameter obtained for the deposit prepared at 800 °C, 0.818038(7) nm, is consistent with others previously reported for spinels of similar composition [23]. The virtual absence of the (2 2 0) reflection is indicative of the prevalence of a normal type structure where 8*a* sites are essentially occupied by Li-ions and octahedral positions (16*d*) by the transition elements. On the other hand, the good correlation between the intensities of the peaks in the XRD patterns of Fig. 2 and those of the ASTM card [24] suggests that particle growth was quite isotropic—the absence of a preferred orientation is a common feature of these deposits.

Fig. 3 shows the variation of the surface morphology with the annealing temperature. At 400 °C, the deposits exhibited an earthworm-like morphology around 4 μm in length and 0.5 μm width, with a gel-like appearance. The formation of a layer of undecomposed organic components coating the spinel particles must be the origin of this peculiar morphology; also, it is consistent with the crystalline nature of the deposit as revealed by the XRD data. On further heating, the worm-like shape gradually disappeared, and at 600 °C, the deposit surface consisted of quasi-spherical submicronic grains. At 800 °C, the particles developed a polyhedral morphology with well-defined edges and faces typical of the spinel-type structure and ranging in size from 0.2 to 0.4 μm. This is consistent with the improved crystallinity revealed by the decreased XRD line width. Fig. 3d shows a SEM image of the cross-section of the deposit of 0.20 mg. The thickness was seemingly quite uniform (∼3 μm). Based on the spinel density (4.4 g cm^{-3}) and the substrate area (1.32 cm^2), a thickness of 0.34 μm (viz. one order of magnitude smaller than that observed by SEM) was calculated. This was a common finding for other films containing variable amounts of spinel deposit.

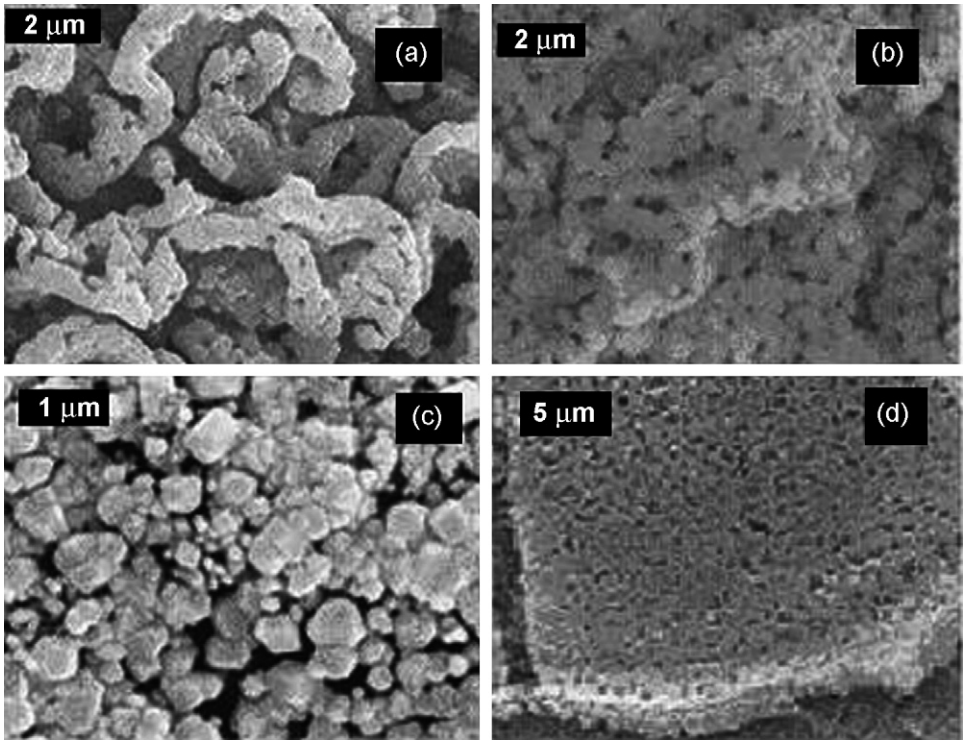

Fig. 3. SEM images of the spin-coating deposits calcined at: (a) 400, (b) 600 and (c) 800 °C. (d) Cross-sectional view of a deposit calcined at 800 °C.

Table 1
Binding energies, in eV, of the C 1s, O 1s and Ni $2p_{3/2}$ emission peaks for the deposit prepared by spin-coating at 800 °C

C 1s	Ni $2p_{3/2}$	O 1s
284.8 (78)	854.1 (78)	529.4 (72)
286.3 (11)	855.7 (22)	530.9 (19)
288.2 (11)		532.1 (6)
		533.1 (3)

The values in brackets are percent peak intensities.

Table 2
Atomic concentration of the elements (%) obtained from XPS data

C	O	Li	Ni	Mn	Au
33.41	40.71	8.02	2.85	14.11	0.88

This means that the deposits were rather porous, as can also be inferred from the top view image of Fig. 3c.

Supplementary information about the different chemical environment of the elements in the spinel and the surface composition was obtained from the high-resolution XPS spectra for O 1s, C 1s, Mn 2p and Ni 2p shown in Fig. 4a–d, and the binding energies (BE) and component proportions listed in Table 1. This study was conducted on the coatings prepared at 800 °C, the particles of which exhibited improved crystallinity and yielded the best electrochemical response as shown below. The atomic concentration found is also included in Table 2. The low intensity/background ratio of the Li 1s emission peak resulting from its low scattering coefficient towards X-rays introduced a significant error in both the element content and its BE. Three findings are worth special note in this context, namely: (i) the appearance of the Au 4f photoemission peak, the atomic concentration of which, consistent with effective coating of the substrate surface was quite low (ca. 1.0%); (ii) the C concentration was rather high, but most C was adventitious carbon, consistent with the presence of the organic precursors in traces amounts and (iii) an Mn/Ni ratio close to five, which is substantially higher than the stoichiometry value (3)—therefore, Mn tends to concentrate at particle surfaces.

The O 1s spectrum exhibited a complex profile with a major component centered at 529.6–529.8 eV that was assigned to Mn(Ni, Li)–O bonds. The components at higher binding energies were of lower intensity and are typically associated to either OH^- groups, O^{2-} or the multiplicity of physisorbed and chemisorbed water on and into the surface [25] or to some O bound to carbon from organic precursor traces. The C 1s spectrum was fitted to three components. The lowest BE component at 284.8 eV was due mainly to adventitious C, whereas the other two corresponded to C bound to O (either through a single bond, peak at 286.3 eV, or carboxylate or carbonate, the latter coming from surface carbonation, peak at 288. 2 eV [26], these components being very small).

The BE value for the Mn $2p_{3/2}$ peak, 642.4 eV, is somewhat higher than those reported for $NiMn_2O_4$ (formally with Mn^{3+} as the main component) [27] and $LiM_{0.2}Mn_{1.8}O_4$ (M = Fe, Co, Ni) [28]. This must be related to the increased content in Mn^{4+} of the spinels as derived from the average oxidation states. Moreover, the absence of the satellite peak clearly observed 5 eV above the $2p_{3/2}$ component [29] for Mn^{2+} rules out the presence of manganese in this oxidation state.

The Ni 2p spectrum, Fig. 4d, was fitted to three components. The signal at 855.1 eV was assigned to Ni^{2+} ions at octahedral sites of the spinel structure and was the main component of the Ni $2p_{3/2}$ emission peak. This value is consistent with those reported for other Ni and Mn spinels (e.g., 855.2 eV for $NiMn_2O_4$) [27], but somewhat higher than that for $LiNi_{0.5}Mn_{1.5}O_4$ (854.3 eV)

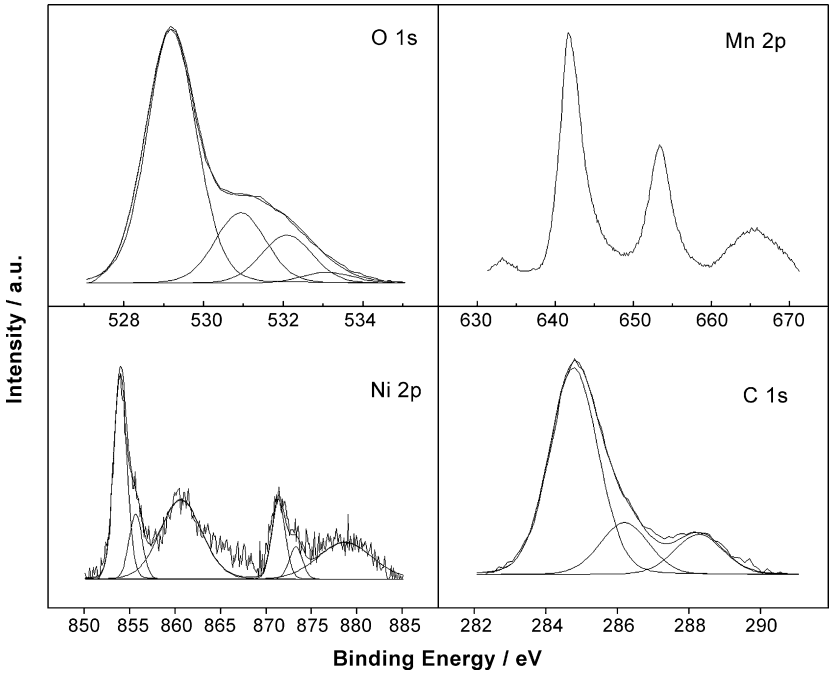

Fig. 4. XPS spectra for the O 1s, C 1s, Mn 2p and Ni 2p regions.

[30]. However, values as low as 852.5 eV have been reported for $Ni_{0.7}Mn_{2.3}O_4$ [31]. Charging effects, among other factors, could be the origin of this difference. The assignation of the peak at 857.0 eV is more uncertain, in fact, the peak can be assigned to both Ni^{3+} cations [30] and surface nickel hydroxide species [32]. However, an Mn/Ni atomic ratio greater than 3.0 is inconsistent with the presence of surface hydroxide as the formation of this species would result in an Mn/Ni ratio lower than the theoretical one. The presence of Ni^{3+} would require an equivalent content of Mn^{3+} in the spinel lattice. This is further confirmed by the electrochemical data. The "shake up" satellite peak centered at 861.5 eV must be due to both types of Ni. The presence of Mn^{3+} has also been ascribed to some defect of oxygen in the structure [33]. However, our experience with bulk spinels prepared from similar precursors is more consistent with a stoichiometric formula in oxygen [34], so we are inclined to relate the presence of Mn^{3+} with Ni^{3+}.

In order to better characterize the film surface, some depth profiles were recorded. Fig. 5 shows the XPS concentrations for carbon, oxygen, manganese, nickel and Au. Carbon was the sole element, the content in which decreased with etching; after few minutes, its concentration fell to nearly negligible values, which suggests that most of the carbon observed was adventitious carbon; this is consistent with virtually complete pyrolysis of the organic precursors. The oxygen concentration barely changed with etching; however, the concentrations of nickel and manganese increased during the first few minutes of etching and then levelled off on prolonged etching. The Au concentration, which, as noted previously, was very low, tended to increase slightly, probably through pickling of the deposit produced by the sputtering process. In summary, a thin layer of carbon coats, the deposit, the presence of which, however, seems to have no adverse effect on its electrochemical properties in lithium cells.

3.2. Electrochemical properties

The electrochemical response of the coating was initially monitored by step potential electrochemical spectroscopy (SPES). Fig. 6 shows the SPES curves for three films prepared at 400, 600 and 800 °C. Although the shape of the curves reveals similar features and essentially reflects the reversibility of the redox reaction involved in the removal and insertion of Li, there are clear differences in the peak intensity. Thus, the anodic scans exhibit two regions of electrochemical activity over the ranges 3.9–4.4 and 4.5–5.0 V, respectively. The former is related to the Mn^{3+}/Mn^{4+} redox couple. The intensity of this broad peak decreased with increasing temperature, so much so that the peak was barely detectable at 800 °C. These means that heating decreased the Mn^{3+} content, as also observed in the bulk spinel [34]. No significant change in the Ni^{2+}/Ni^{3+} ratio in the XPS spectra on heating was observed. Thereby, the decrease in Mn^{3+} content must be associated with oxidation of this element as the calcining temperature is raised. Electrochemical activity occurs mainly in the 4.7–5.0 V region, where a double peak associated to the $Ni^{2+} \rightarrow Ni^{4+}$ process, the mechanism of which reportedly involves two cubic/cubic two-phase reactions [35], appears. Also, based on spectroscopic results [36], the oxidation of Ni^{2+} to Ni^{4+} takes place via the following reactions involving the formation of Ni^{3+} as an intermediate species:

$$\begin{aligned} Li[Ni(II)_{0.5}Mn(IV)_{1.5}]O_4 \rightarrow\ & Li_{0.5}[Ni(III)_{0.5}Mn(IV)_{1.5}]O_4 \\ & + 0.5Li^+ + 0.5e^- \rightarrow [Ni(IV)_{0.5}Mn(IV)_{1.5}]O_4 + 0.5Li^+ \\ & + 0.5e^- \end{aligned} \quad (1)$$

This process is reversible and the calcination temperature affects the shape of the curve rather than its area, which is consistent with the preservation of the Ni^{2+}/Ni^{3+} ratio. Increasing the temperature alters the curve shape in two respects, mainly: (i) it sharpens both peaks, which is consistent with an increase in the rate of lithium insertion and extraction and (ii) it results in a more pronounced current drop after the higher voltage peak in

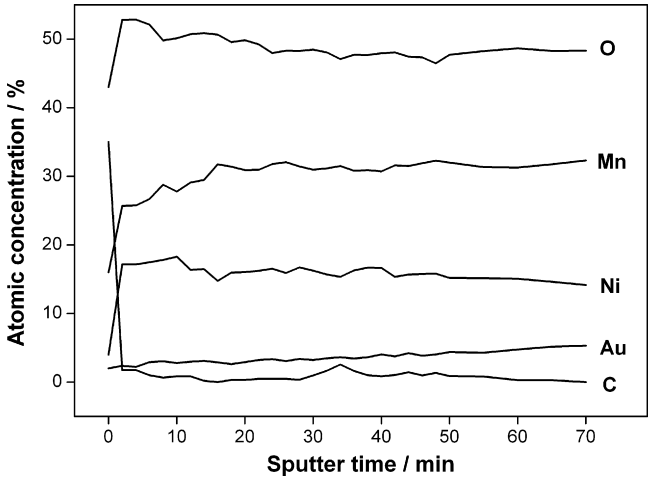

Fig. 5. XPS depth profiles for a spin-coating deposit calcined at 800 °C.

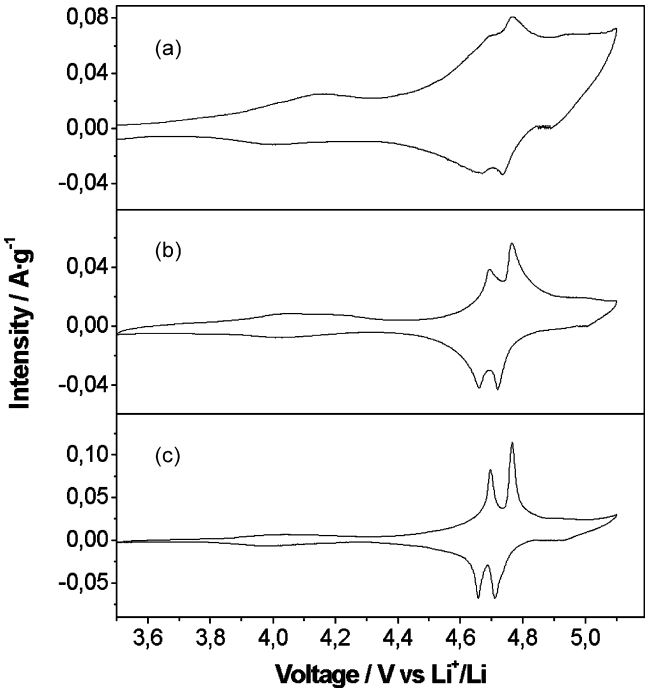

Fig. 6. SPES curves for the spin-coating deposits calcined at: (a) 400, (b) 600 and (c) 800 °C.

Table 3
Charge/discharge capacity values ($Ah\,kg^{-1}$) obtained from the SPES curves

Cycle	Charge	Discharge
First	176.5	59.5
Second	163.2	66.8
Third	161.0	68.6
Fourth	148.6	70.9
Fifth	137.0	73.2

Coating calcined at 800 °C.

the anodic scan. Both results can be associated to the improved crystallinity of the deposits on heating. On the other hand, the persistence of some current above the high-voltage peak, particularly the coating prepared at 400 °C, can be ascribed to the release of oxygen, which increases with increasing lattice disorder [37].

The charge/discharge capacities values obtained from the SPES curves are shown in Table 3. These data correspond to the coating prepared at 800 °C, which proved the best electrochemical performer. As can be seen, its charge capacity nearly trebled the discharge capacity; also, it deviated from the theoretical capacity (ca. 148 $mAh\,g^{-1}$ based on the $LiNi_{0.5}Mn_{1.5}O_4$ stoichiometry) in the three first cycles. The origin of this difference, and especially, the overcharge observed, is unclear as discussed below. These results differ from those reported for $LiNi_{0.5}Mn_{1.5}O_4$ deposited by electrostatic spraying on gold substrates but analyzed by cyclic voltammetry [21]. The electrode, made from 0.097 $mg\,cm^{-2}$, delivered a capacity very close to the theoretical value.

The cycling properties of the cell were tested galvanostatically over the range 3.5–5.0 V and at a C/2 rate. Based on the potentiostatic data, only the coatings calcined at 800 °C were examined under this regime. Fig. 7 shows the charge/discharge curves for some of the 50 cycles. The most salient feature of the charge curve is the presence of two well-defined pseudo-plateaux in the 4.6–4.8 V region consistent with the two peaks of the SPES curve (Fig. 6c). A small inflection centred at ca. 4.2 V is also present that is associated with the oxidation of a small fraction of Mn^{3+} to Mn^{4+}. This confirms that the average coating stoichiometry is close to $LiNi_{0.5}Mn_{1.5}O_4$. The slope of the curve above 4.8 V can be ascribed to the release of some oxygen from the spinel framework. The discharge curves were similar to those for the charge process and exhibited two well-defined plateaux over the range 4.5–4.8 V that can be ascribed to the reduction of Ni^{4+} to Ni^{2+}, and is followed by a short plateau at around 4.0 V that accounts for the reduction of Mn^{4+} to Mn^{3+}. All these features were retained over a large number of cycles, which confirms the electrochemical reversibility of the lithium insertion/deinsertion reaction in the coatings. The shape of the differential charge/discharge capacity curves after 50 cycles (see inset in Fig. 7) is similar to that of the SPES curves, Fig. 6c; also, they exhibit two well-resolved peaks in the 4.5–5.0 V region that are consistent with the reversibility of reaction (1) and the retention of the spinel structure on prolonged cycling. Again, the charge curve was much longer than the discharge curve, so the electrode was significantly overcharged under a galvanostatic regime.

The origin of the overcharge was additionally studied in two tests. One was intended to clarify the role played by the substrate in the side reaction (viz. an electrolyte decomposition catalyzed by gold). Fig. 8 shows the first charge/discharge curves for the cell made from uncoated substrate. On charging the cell, a pseudo-plateau was observed in the region of 4.5–5.0 V (the same where the oxidation peak for Ni^{2+} appears). The oxidation of gold as the origin of this reaction is ruled out because it is irreversible as revealed the discharge curve strongly polarized. Thus, the electrochemical reaction might affect to the electrolyte oxidation probably catalyzed by the gold surface. The extent of such a reaction, that decreased on further cycling, was difficult to quantify because the difficulty to know the amount of active electrolyte in the electrochemical reaction and the final reaction products. Anyway, this test demonstrates that the substrate was sensitive to the electrolyte decomposition; however, how the extent of reaction could be quantified remains unclear.

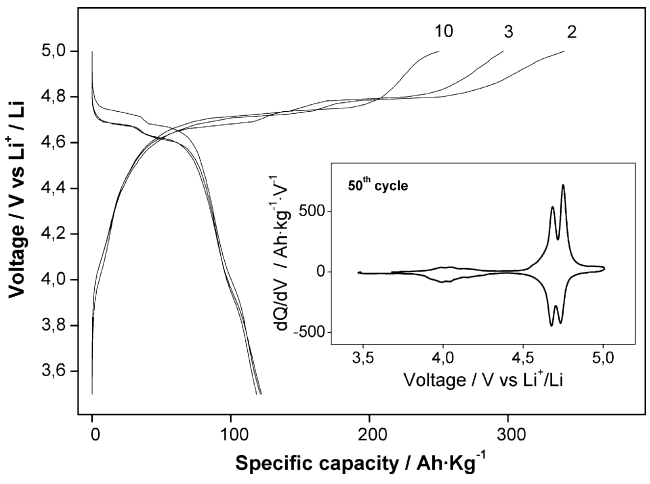

Fig. 7. Galvanostatic charge–discharge curves for a spin-coating deposit (0.066 $mg\,cm^{-2}$) cycled over the voltage range 3.5–5.0 V. The inset shows the differential capacity for the cell at the 50th cycle.

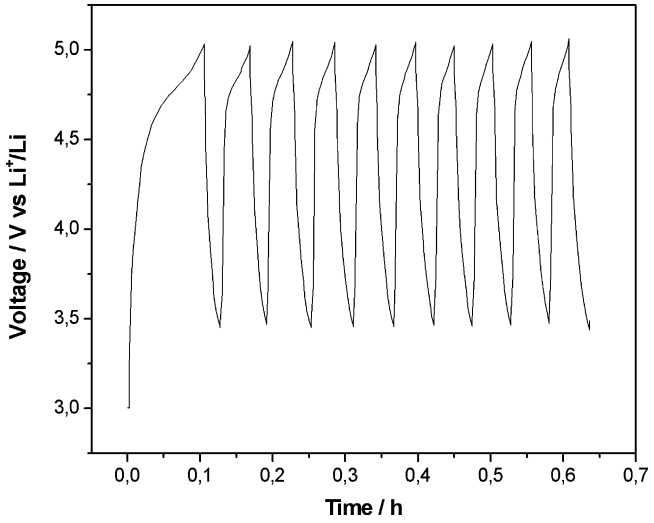

Fig. 8. Galvanostatic curves for an Au/electrolyte/Li cell. Voltage range 3.5–5.0 V.

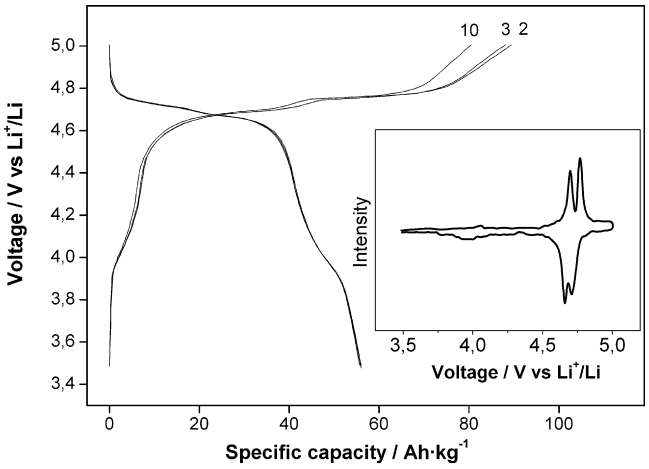

Fig. 9. Galvanostatic charge–discharge curves for a spin-coating deposit (0.331 mg cm^{-2}) cycled over the voltage range 3.5–5.0 V. The inset shows the cyclic voltammetric curve.

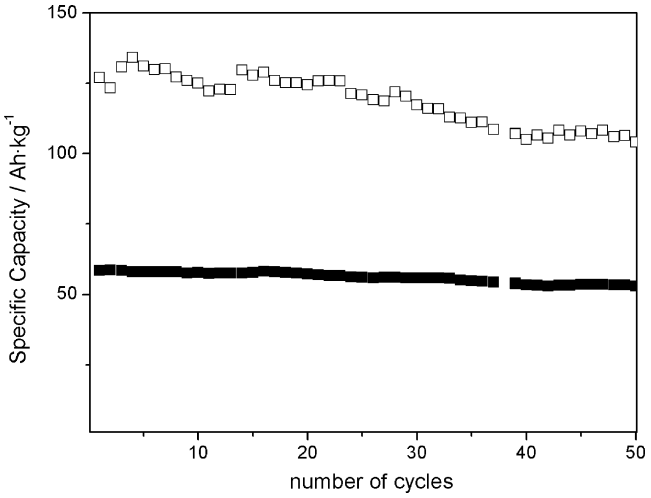

Fig. 10. Variation of the capacity delivered by the cells as a function of the number of cycles. Amount deposited: 0.066 (□) and 0.331 mg cm^{-2} (■).

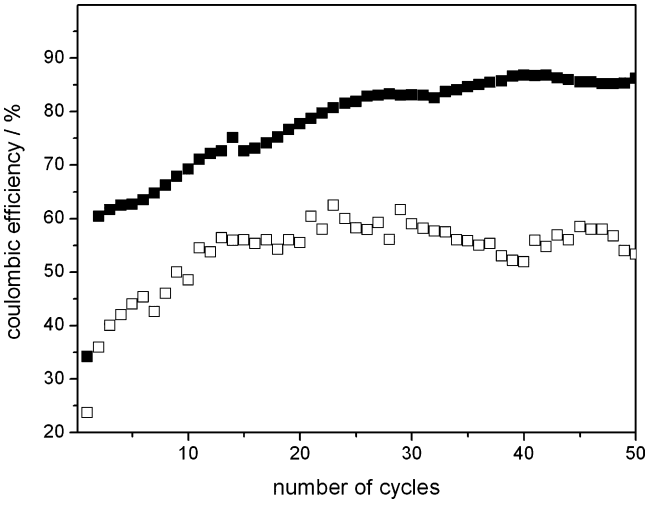

Fig. 11. Variation of the coulombic efficiency as a function of the number of cycles. Amount deposited: 0.066 (□) and 0.331 mg cm^{-2} (■).

For the second test, we selected two electrodes of different load, 0.066 mg cm^{-2} – the electrochemical properties of which have been commented above (see Fig. 7) – and 0.331 mg cm^{-2}. Although the shape of the charge and discharge curves for the two deposits, Figs. 7 and 9, reflected the principal electrochemical characteristics of the spinel (viz. the presence of two pseudo-plateaux and two peaks in the 4.5–4.9 V range for the galvanostatic and cyclic voltammetric curves, respectively), there were two differences worth note, one in the overcharge values and the other in the capacities delivered by the cells. Thus, the thinner electrode produced significant overcharge (more than three times the capacity delivered in the first few cycles). Although, the overcharge was markedly reduced on increasing the electrode thickness, Fig. 9, it exceeded that of the bulk spinel [38]. Concerning the capacity delivered by the cell, the thinner deposit was capable of delivering 130 mAh g^{-1}, a value somewhat lower than that estimated from the spinel stoichiometry. Moreover, the cell exhibited an acceptable capacity retention in successive cycles (it decreased to 105 mAh g^{-1} at the 50 cycle, see Fig. 10). Cells with thicker coatings also retained most of their capacity, at the expense of a marked decrease in the delivered capacity (more than a 50%). However, the coulombic efficiency (Fig. 11) was higher for the thicker electrode and approached 85% after prolonged cycling (versus 55% for the thinner electrode). An increased thickness probably hinders contact between the electrolyte and substrate, thus, decreasing the overcharge and increasing the coulombic efficiency. In any case, the value of this parameter is smaller than that obtained for the cell made from the bulk spinel using a steel grid as current collector [38], which suggests the involvement of gold in the electrochemical process.

The decreased capacity delivered by the cells made from the thicker electrodes can be ascribed to at least two factors, namely: the absence of carbon to improve the electronic conductivity of the electrode and the decrease in interparticle connectivity with increasing deposit thickness, typical of porous deposits (see Fig. 2). In fact, $LiNi_{0.5}Mn_{1.5}O_4$ is a poor semiconductor owing to the lack of Mn^{3+}, which hinders the electron hopping mechanism and causes a significant decrease in electronic conductivity relative to the $LiMn_2O_4$ spinel [39]. New experiments in progress will hopefully reduce the overcharge observed on charging the cell and result in improved electrode performance irrespective of the particular coating thickness. Special attention will be paid to the use of alternative electrolytes, such as lithium a bis(oxalate)borate (LiBOB)-based electrolyte which has exhibited quite attractive properties at high potentials and temperatures [40].

4. Conclusions

Spin-coating methodology is an effective tool for preparing homogeneous deposits of $LiNi_{0.5}Mn_{1.5}O_4$ spinel by using an appropriate solvent precursor to wet the substrate. Ensuring good electrochemical performance requires a high crystallinity that can be achieved by calcining at high temperatures (e.g., 800 °C). This precludes the use of substrates, such as stainless steel because it undergoes surface deterioration at high temperatures. Gold is a good choice for preparing deposits of highly

purity crystallinity in addition to a well-defined particle shape. When use as electrodes in lithium cells, these deposits react reversibly with lithium upon extended cycling, but are subject to two major problems, namely: (i) a high overcharge that results in low coulombic efficiencies (particularly in the first few cycles), the overcharge being ascribed to the electrolyte decomposition above 4 V catalyzed by gold and (ii) the dependence of the capacity delivered by the cell on the coating thickness. Thus, at a low thickness, the capacity was similar to that estimated from the spinel stoichiometry (around 148 mAh g^{-1}); at higher ones, however, the capacity was significantly reduced. This may have resulted from degraded electronic conductivity – these deposits contain no additive conductors, such as carbon, so particles are loosely bound – reducing the mobility of charge carriers.

Acknowledgements

This work was supported by Junta de Andalucía (Group FQM-175) and Spain's Ministerio de Ciencia y Tecnología (Project MAT2002-04477-C02-02).

References

[1] N.J. Dudney, B.J. Neudecker, Solid-State Mater. Sci. 4 (1999) 479.
[2] Y.S. Park, S.H. Lee, B.I. Lee, S.K. Joo, Electrochem. Solid State Lett. 2 (1999) 58.
[3] B.J. Neudecker, N.J. Dudney, J.B. Bates, J. Electrochem. Soc. 147 (2000) 517.
[4] J.L. Souquet, M. Duclot, Solid State Ionics 148 (2002) 375.
[5] I. Taniguchi, D. Song, M. Wakihara, J. Power Sources 109 (2002) 333.
[6] W.G. Lee, R.L. Smith, J. Electrochem. Soc. 152 (2005) A1054.
[7] P. Liu, J.G. Zhang, J.A. Turner, C.E. Tracy, D.K. Benson, J. Electrochem. Soc. 146 (1999) 200.
[8] M.M. Thackeray, M.F. Mansuetto, J.B. Bates, J. Power Sources 68 (1997) 153.
[9] Y.I. Jang, N.J. Dudney, D.A. Bloom, L.F. Allard, J. Electrochem. Soc. 149 (2002) A1442.
[10] S.I. Cho, S.G. Yoon, J. Electrochem. Soc. 149 (2002) A1584.
[11] K.F. Chiu, H.H. Hsiao, G.S. Chen, H.L. Liu, J.L. Her, H.C. Lin, J: Electrochem. Soc. 151 (2004) A452.
[12] S.W. Jeon, J.K. Lim, S.W. Lim, S.M. Lee, Electrochim. Acta 51 (2005) 268.
[13] T. Fukutsuka, K. Sakamoto, Y. Matsuo, Y. Sugie, T. Abe, Z. Ogumi, Electrochem. Solid State Lett. 7 (2004) A481.
[14] Y.H. Rho, K. Kanamura, T. Umegaki, J. Electrochem. Soc. 150 (2003) A107.
[15] A. Würsig, H. Buqa, M. Holzapfel, F. Krumeich, P. Novak, Electrochem. Solid State Lett. 8 (2005) A34.
[16] C. Sigala, D. Guyomard, A. Verbaere, Y. Piffard, M. Tournoux, Solid Sate Ionics 81 (1995) 167.
[17] Q. Zhong, A. Bonakdarpour, M. Zhang, Y. Gao, J.R. Dahn, J. Electrochem. Soc. 144 (1997) 205.
[18] H. Kawai, M. Nagata, H. Tukamoto, A.R. West, Chem. Mater. 10 (1998) 3266.
[19] J.H. Kim, A.T. Myung, Y.K. Sun, Electrochim. Acta 49 (2004) 219.
[20] K. Takahashi, M. Saitoh, M. Sano, M. Fujita, K. Kifune, J. Electrochem. Soc. 151 (2004) A173.
[21] M. Mohamedi, M. Makino, K. Dokko, T. Itoh, I. Uchida, Electrochim. Acta 48 (2002) 79.
[22] A. Caballero, L. Hernán, M. Melero, J. Morales, R. Moreno, B. Ferrari, J. Power Sources 158 (2006) 583.
[23] Y. Ein-Eli, J.T. Vaughey, M.M. Thackeray, S. Mukerjee, X.Q. Yang, J. McBreen, J. Electrochem. Soc. 146 (1999) 908.
[24] Diffraction Data File No. 32-0581, ICDD International Center for Diffraction Data, Pennsylvania, USA, 1991.
[25] T. Choudhury, S.O. Saied, J.L. Sullivan, A.M. Abbot, J. Phys. D: Appl. Phys. 22 (1989) 1185.
[26] H. Takezawa, K. Kanamura, S. Shiraishi, Z.I. Takehara, J. Electrochem. Soc. 144 (1997) 1900.
[27] J.F. Moulder, W.F. Stickle, P.E. Sool, K.D. Bomber, Handbook of X-ray Photoelectron Spectroscopy, Perkin-Elmer, Eden Prairie, 1992.
[28] L. Hernán, J. Morales, L. Sánchez, E. Rodríguez Castellón, M.A.G. Aranda, J. Mater. Chem. 12 (2002) 734.
[29] A.E. Bocquet, T. Mizokawa, T. Saitoh, H. Namatame, A. Fujimori, Phys. Rev. B 46 (1992) 3777.
[30] K. Amine, H. Tukamoto, H. Yasuda, Y. Fujita, J. Electrochem. Soc. 143 (1996) 1607.
[31] C. Drouet, C. Laberty, J.L.G. Fierro, P. Alphonse, A. Rousset, Int. J. Inorg. Mater. 2 (2000) 419.
[32] J.F. Marco, J.R. Gancedo, M. Gracia, J.L. Gautier, E. Rios, F.J. Berry, J. Solid State Chem. 153 (2000) 74.
[33] J.H. Kim, S.T. Myung, C.S. Yoon, S.G. Kang, Y.K. Sun, Chem. Mater. 16 (2004) 906.
[34] A. Caballero, M. Cruz, L. Hernán, M. Melero, J. Morales, E. Rodríguez Castellón, J. Electrochem. Soc. 152 (2005) A552.
[35] K. Ariyoshi, Y. Iwakoshi, N. Nakayama, T. Ohzuku, J. Electrochem. Soc. 151 (2004) 296.
[36] T. Terada, K. Yasaka, F. Nishikawa, T. Konishi, M. Yoshio, I. Nakai, J. Solid State Chem. 156 (2001) 281.
[37] A. Caballero, L. Hernán, M. Melero, J. Morales, M. Angulo, J. Electrochem. Soc. 152 (2005) A6.
[38] J.C. Arrebola, A. Caballero, L. Hernán, J. Morales Electrochem. Solid-State Lett. 8 (2005) A641.
[39] M.G. Lazarraga, L. Pacual, H. Gadjov, D. Kovacheva, K. Petrov, J.M. Amarilla, R.M. Rojas, M.A. Martín-Luengo, J.M. Rojo, J. Mater. Chem. 14 (2000).
[40] S.S. Zhang, K. Xu, T.R. Jow, J. Power Sources 154 (2006) 276.